Progress In Electromagnetics Research C, Vol. 102, 63–77, 2020

Compact Two-Port MIMO Antenna with High Isolation Using Parasitic Reflectors for UWB, X and Ku Band Applications

Tathababu Addepalli[1, *] and Vaddinuri R. Anitha[2]

Abstract—In this communication, a compact two-port multiple input multiple output (MIMO) antenna with high isolation is presented for multiband applications. The size of the proposed structure is $0.15\lambda_0 \times 0.27\lambda_0$ (λ_0, measured at lower frequency, is 2.95 GHz), and the antenna elements are separated by a distance of $0.04\lambda_0$. The truncated partial ground offers good impedance performance with a fractional bandwidth of 136.5% from 2.95 to 15.65 GHz and covers the uninterrupted ultra-wideband (UWB), X and Ku band applications. High isolation of more than 25 dB is attained by placing parasitic elements between the antennas in a precise manner. The proposed structure is simulated, fabricated, tested, and verified practically. The radiation efficiency is more than 90% of the entire band. The peak gain values vary from 1.2 to 6.8 dB in the desired band, and its maximum value is 6.8 dB at 11.6 GHz. Diversity performance is also studied. The proposed structure offers an envelope correlation coefficient (ECC) of less than 0.04, diversity gain (DG) of greater than 9.996 dB, total active reflection coefficient (TARC) of below −10 dB, mean effective gain (MEG) of around −3 dB, and channel capacity losses (CCL) values are below 0.2 bits/sec/Hz. The measured and simulation results are in good concord.

1. INTRODUCTION

Multiple input multiple output (MIMO) technology plays a key role in present wireless communications due to its features like higher data rate, more channel capacity than single element system, high signal to noise ratio (SNR), good quality of transmission, excellent diversity performance and more reliability without the need for additional transmitter power and bandwidth. In MIMO technology, multiple antennas are placed side by side at the transmitting and receiving ends. Due to the small space between antenna elements in portable devices, mutual coupling is introduced, which degrades the system performance. Hence, coupling is a primary limiting factor in MIMO technology [1]. In 2002, the Federal Communications Commission (FCC) assigned an unlicensed band from 3.1 to 10.6 GHz named ultra-wideband (UWB). However, UWB system suffers from signal (multipath) fading in a multipath environment. The MIMO technology effectively mitigates the fading problem using diversity techniques like spatial multiplexing and space-time coding. The combination of UWB with MIMO technology has more applications in wireless technology due to its wide bandwidth and high diversity performance, but it is still agonized with the coupling problem.

The review of several techniques for isolation enhancement (or mutual coupling reduction) between antenna elements in MIMO systems is discussed in [2]. In addition, various decoupling structures were presented in [3–27] such as novel printed circuit structures [3], wideband planar structure [4], defected ground structure loaded with meandered lines [5], miniature double-layer EBG structure [6], the orthogonal arrangement of a modified rectangular shaped radiators [7], fence type decoupling structure [8], and metamaterial-based structure [9]. Also, the isolation is improved

Received 4 March 2020, Accepted 29 April 2020, Scheduled 18 May 2020
* Corresponding author: Tathababu Addepalli (babu.478@gmail.com).
[1] Department of ECE, JNTUA, Ananthapur, A.P, India. [2] ECE, Antenna Research Lab, Sree Vidyanikethan Engineering College, Tirupathi, A.P, India.

between radiating elements using F-shaped stubs placed between elements [10], resistive loading [11], a quasi self-complementary arrangement of antenna elements [12], two meandering monopoles using inverted L-shaped stubs [13], wideband neutralization line [14], and a modified T-shaped stub [15]. Other decoupling structures have been discussed which include protruded parasitic stubs between MIMO antenna elements [16–18], double grounded CRR structure between semi-hexagonal-shaped ring antennas [19], a T-shaped slot in the ground plane [20], a simple ground stub between linearly polarized monopoles [21], a rectangular-shaped ground plane with an extruded T-shaped stub [22], inserting two inverted L-shaped stubs on the ground plane [23], using polarization diversity and ground slots [24], adopting T-stepped ground stub [25], a Y-shaped slot cut at the bottom center of the common ground plane [26], and two inverted L-strips are loaded over a conventional rectangular patch antenna [27]. The antennas discussed in [3–27] have acceptable bandwidth and isolation. Still, most of the designs are not enough compact to fit into the portable devices, and the isolation techniques are a bit complex. Hence, there is a scope for a compact MIMO antenna with high isolation.

In this paper, a simple and compact UWB-MIMO antenna with high isolation using parasitic reflectors is presented. The overall size of the proposed MIMO antenna is $0.15\lambda_0 \times 0.27\lambda_0$ ($16 \times 28\,\text{mm}^2$), and the antenna elements are separated by a distance of $0.04\lambda_0$ (4 mm). The truncated partial ground provides good impedance performance, and high isolation is achieved by placing parasitic reflectors between the elements. The proposed antenna is also studied by changing the ground length, major axis, and the axial ratio of the antenna element, feed width, and the antenna adjacent parasitic element. The positions of parasitic elements are also essential for isolation improvement. The proposed design achieves wide impedance bandwidth from 2.95 to 15.65 GHz and isolation above 25 dB throughout the band. The advantages of the proposed antenna are compact size, high isolation, high radiation efficiency, good peak gain values, low ECC, high DG values, good TARC values, acceptable MEG values, and low CCL values.

2. ANTENNA DESIGN AND ANALYSIS

The proposed compact structure is designed and simulated using ANSYS HFSS Electronics Desktop 16.2 simulator. The structure is fabricated on a low-cost FR4 material which has relative permittivity (ε_r) of 4.4 and loss of tangent 0.02. The designed antenna consists of two elliptical-shaped monopole antennas which are separated by parasitic elements. The geometry of the proposed structure is as shown in Figure 1 with the optimization values $L = 16$ mm, $W = 28$ mm, $S = 4$ mm, ellipse major axis ($M.A$) = 5.8 mm, ellipse axial ratio ($A.R$) = 0.95, $Lg = 3$ mm, $Lf = 7$ mm, $Wf = 1.9$ mm, $A = 10$ mm, $B = 12$ mm, $C = 14$ mm, $D = 0.3$ mm, $E = 2.38$ mm, and $F = 2.6$ mm.

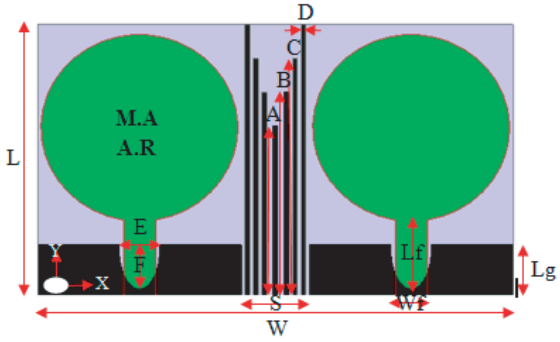

Figure 1. Proposed structure geometry.

The evolutionary stages of the proposed structure are described in Figure 2, and the S-parameters are depicted in Figure 3. In stage 1 (Antenna I), an elliptical-shaped monopole antenna is designed using basic elliptical radiator equations [28]. Due to the compactness of elliptical radiator, partial ground plane, feed width, and substrate dimensions, the antenna resonates from 3.95 GHz to 13.5 GHz with '$S11$' value of −22.8 dB at 5.45 GHz. However, Antenna I does not cover the lower UWB as

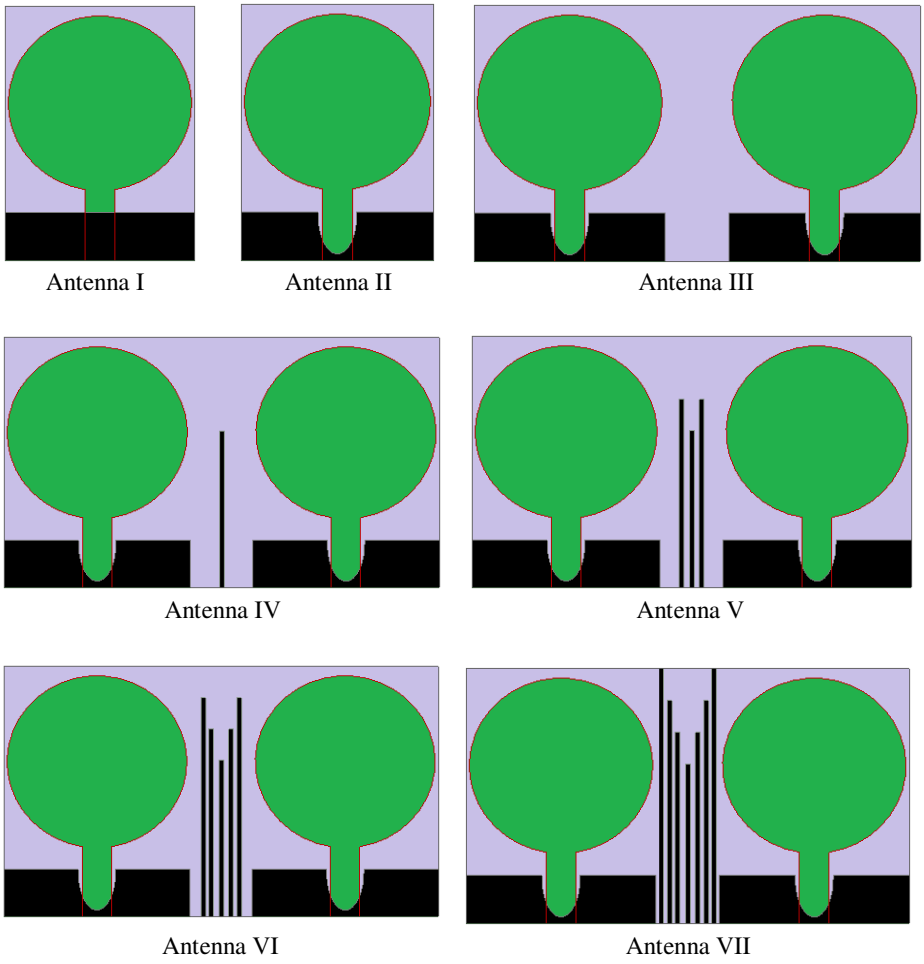

Figure 2. Proposed structure evolution stages.

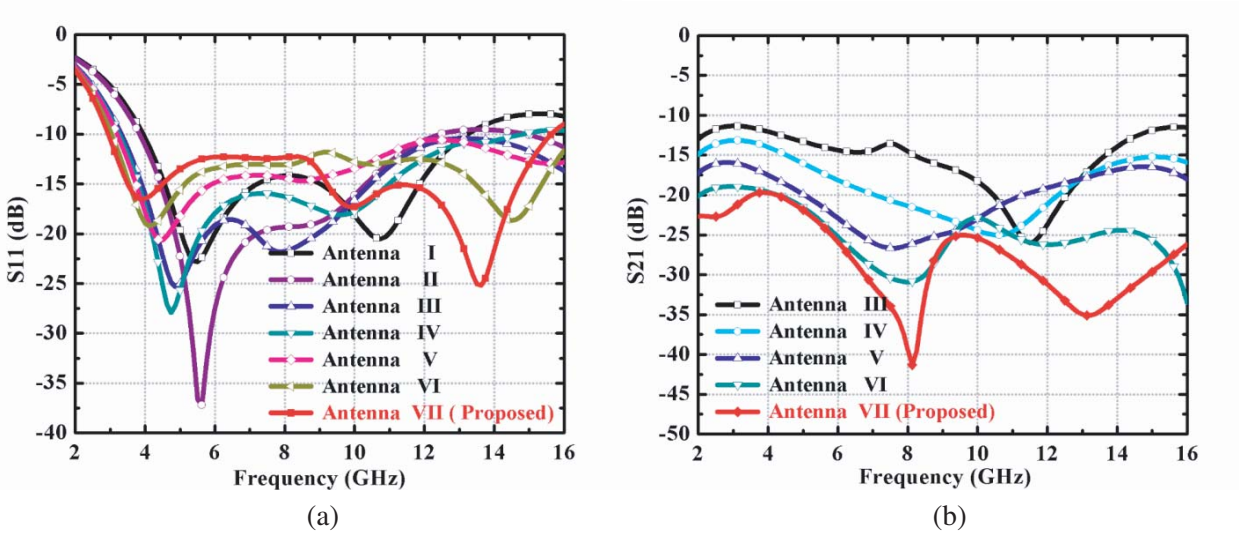

Figure 3. (a) '$S11$' values of evolution stages of proposed structure; (b) '$S21$' values of evolution stages of proposed structure.

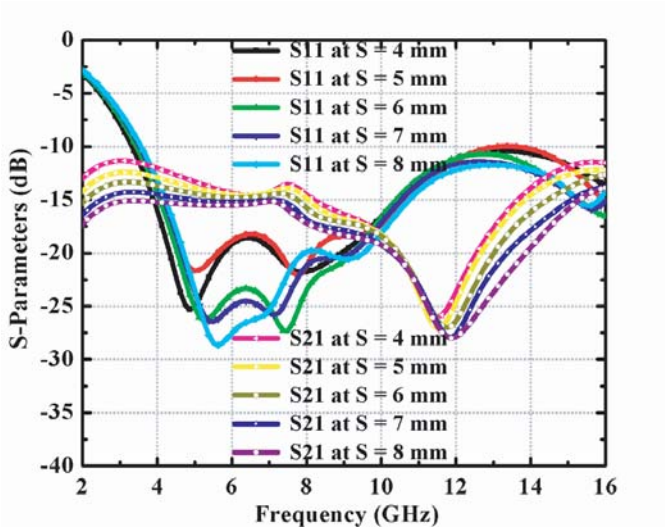

Figure 4. Proposed structure '$S11$' and '$S21$' values with various 'S' values.

observed from Figure 3(a). So, to get impedance matching between the antenna element and port, a small half of the elliptical-shaped strip is removed from the center of the ground in stage 2 (Antenna II) which results in small improvement in the impedance bandwidth from 3.85 to 14.45 GHz with '$S11$' of -37.8 dB at 5.6 GHz. In stage 3 (Antenna III), another ellipse-shaped monopole antenna is placed at a distance of 4 mm from the first element to form a MIMO antenna. The isolation of Antenna III is analyzed for different lengths such as 4 mm, 5 mm, 6 mm, 7 mm, and 8 mm. The variation of '$S11$' and '$S21$' values of the MIMO structure with changes in distance S are as shown in Figure 4. It is observed from Figure 4 that as the distance between elements is decreased, the isolation is reduced, but the lower cutoff frequency is moved to a lower value. At $S = 4$ mm, the lower band value is moved to 3.31 GHz due to reflections between elements, and the isolation above 11.3 dB is obtained in the entire band.

To enhance the isolation, a small strip (10 mm $\times$ 0.3 mm) is placed between the elements in stage 4 (Antenna IV), which results in the isolation of more than 13 dB. Later in stage 5 (Antenna V), the isolation of greater than 16 dB is achieved by including two parallel strips of dimensions 12 mm $\times$ 0.3 mm beside the small strip. In stage 6 (Antenna VI), two more strips are placed, which give rise to the isolation of higher than 19 dB for the entire band. Finally, the proposed antenna, as displayed in stage 7 (Antenna VII), is obtained by adding two parallel strips of size 16 mm $\times$ 0.3 mm at the abreast of the strips of Antenna VI. The results in Figure 3(b) show that isolation is greatly improved to more than 25 dB. These strips give good impedance matching and good isolation between elements. The proposed structure covers the entire UWB band, X band, and Ku band applications. Figure 5 illustrates the surface current distribution of Antenna-III to Antenna VII when port 1 is excited. It is observed from the figure that there is a significant improvement in the isolation of currents from port 1 to port 2 when the inclusion of strips is increased.

The parametric study of the ellipse-shaped monopole antenna parameters such as major axis ($M.A$) & axial ratio ($A.R$), ground length, feed width, and parasitic strip length has been done for the optimal values of the proposed structure which is shown in Figure 6. The antenna is analyzed for the values: $M.A = 5.7$ to 5.9 mm and $A.R = 0.9$ to 1.0 mm, $Lg = 2$ to 4 mm, $Wf = 1.6$ to 2.2 mm, and strip length = 12 to 16 mm. The partial ground plane with a truncated structure gives wider bandwidth. The width of the feed plays a key role in impedance matching between port and antenna. As identified from the figure, the desired performance is achieved for the following optimized values: $M.A = 5.8$ mm, $A.R = 0.95$ mm, $Lg = 3$ mm, $Wf = 1.9$ mm, and strip length = 16 mm, and hence are adopted in this work. The effect of elliptical cutting in the ground on impedance matching is also studied and is presented in Figure 7.

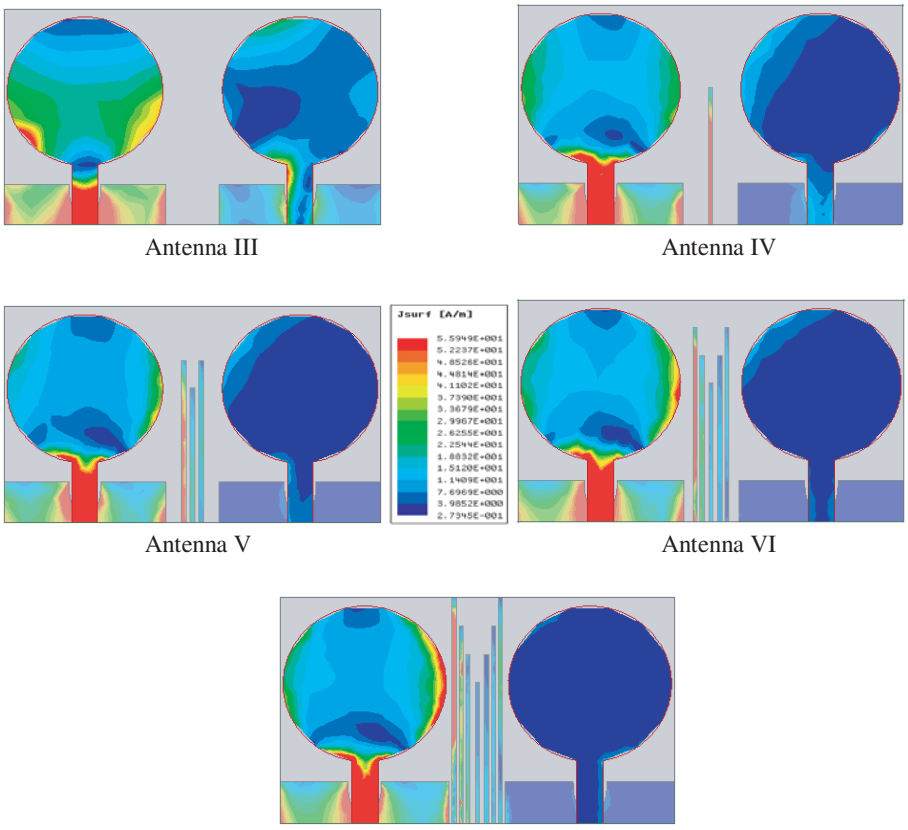

Figure 5. Surface current distribution of the evolution stages of the proposed structure, when port 1 is excited.

3. RESULTS AND DISCUSSIONS

3.1. Impedance Performance

The proposed structure is simulated and fabricated, and the parameters are measured. The '$S11$', '$S22$', '$S12$', and '$S21$' values of the fabricated prototype are measured using a vector network analyzer (Agilent N5224A). Figure 8 describes the S-parameters of the simulated and fabricated antennas. It is observed that the proposed design operates from 2.95 GHz to 15.65 GHz with resonances at 3.8 GHz, 10.0 GHz, and 13.6 GHz. The measured and simulated results are in good agreement except small deviations due to dielectric losses, conducting losses, tolerances in the soldering and fabrication process. Figure 9 shows the radiation efficiency and peak gain values of the proposed structure. The radiation efficiency of an antenna mainly depends on impedance matching between the port and an antenna element. It is identified that the proposed structure offers high efficiency values between 90 and 97%. The high efficiency antennas are used for rectifying antenna (Rectanna) applications. Also, the peak gain values vary from 1.2 to 5.3 dB in respective bands, and the maximum is 6.8 dB at 11.6 GHz.

The impedance bandwidth of the proposed structure without any parasitic elements is only 3.32–13.2 GHz, and isolation is more than 11.3 dB in the entire band. After placing parasitic strips, the bandwidth is improved to 2.95–15.65 GHz and isolation to above 25 dB in most of the band. Hence, the strips are used for impedance matching and isolation enhancement. Figure 10 illustrates the function of the parasitic strip as a reflector. The surface current distribution and 3-D polar radiation patterns with strips, when port 1 is excited and port 2 terminated and vice-versa, are shown in the same figure. It is seen that the parasitic strips act as reflectors by stopping the surface currents entering from one antenna to another antenna. The middle plots in Figure 10 are 3-D polar radiation patterns of the proposed structure without parasitic strips. The remaining two plots in Figure 10 (left and right) represent the

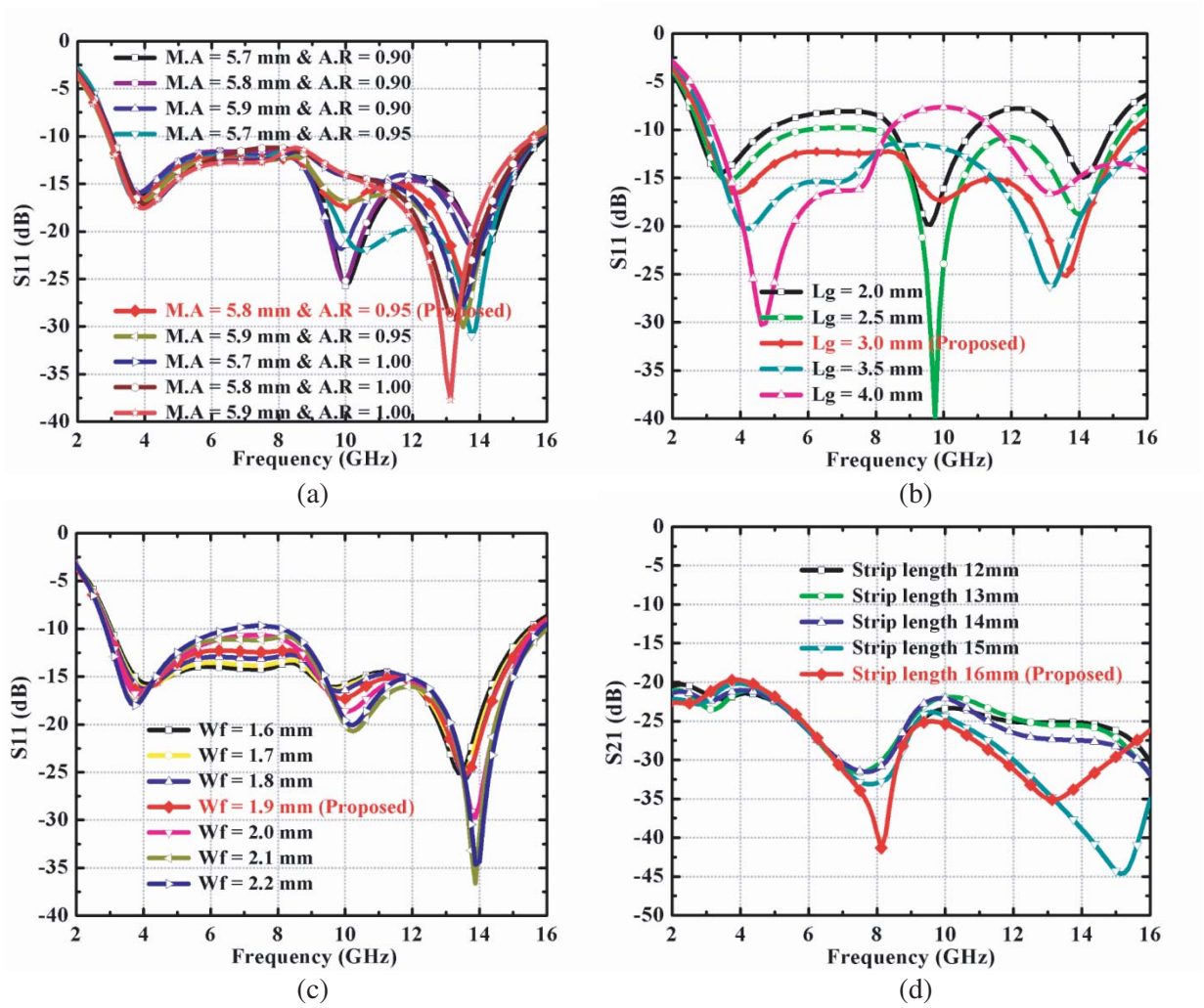

Figure 6. (a) Parametric analysis of major axis and axial ratio; (b) Parametric analysis of ground length; (c) Parametric analysis of feed width; and (d) Parametric analysis of strip length.

effect of strips on radiation pattern and stopping the surface currents when port 1 and port 2 are excited with 50 Ω strip lines, respectively.

3.2. Radiation Performance

The radiation patterns of the proposed structure are measured in an anechoic chamber. The horn antenna is used as a reference antenna, and the proposed structure is used as an antenna under test. Figure 11 illustrates the simulated and measured 2-D radiation patterns (E and H fields) at various frequencies like 3.8 GHz, 6.0 GHz, 8.0 GHz, 10.0 GHz, and 13.6 GHz in the desired band. It is found that the E and H patterns are bidirectional and omnidirectional, respectively. But at higher frequencies, i.e., at 13.6 GHz, the energy will be distributed to all the modes. Hence, the patterns are disturbed at higher bands.

4. MIMO ANTENNA PERFORMANCE

To investigate the diversity performance of the MIMO antenna, metrics like ECC, DG, TARC, MEG, and CCL are required. The ECC has interpreted the correlation between the channels and will give the

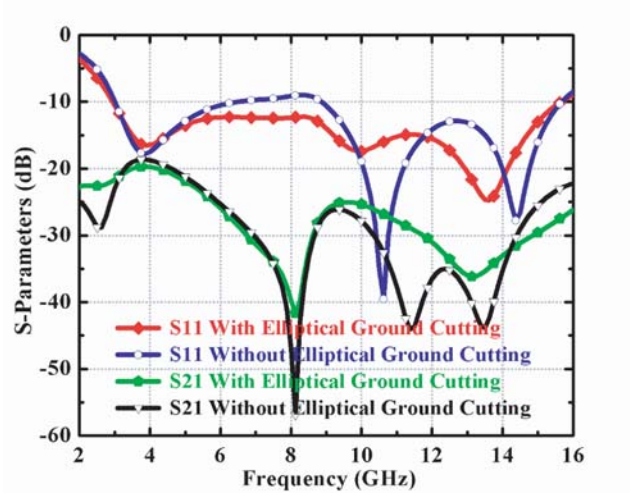

Figure 7. Effect of elliptical cutting in ground on impedance matching.

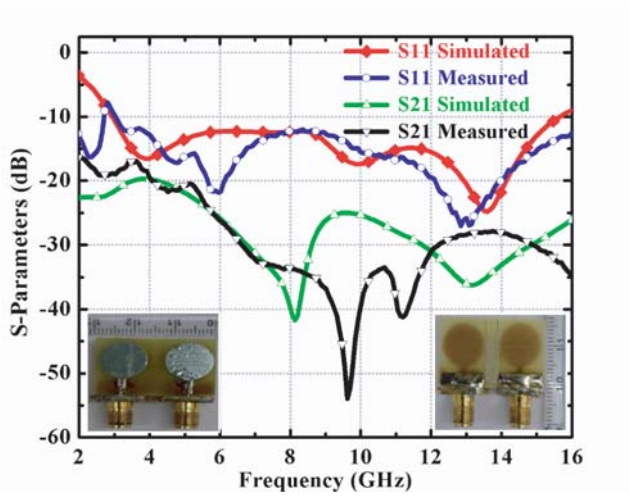

Figure 8. Simulation and measurement S-parameters results.

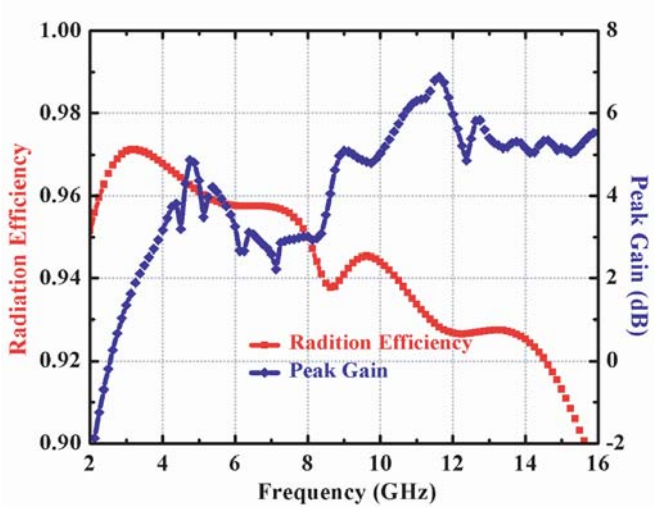

Figure 9. Simulated radiation efficiency and peak gain results.

spatial distribution of signal power in an outdoor environment. ECC is measured in different methods like using S-parameter values, radiation patterns, both S-parameters and radiation efficiencies, and equivalent circuits [29]. Low correlation values indicate good diversity performance. The measurement of ECC using S-parameters is a simple and easy technique. The ECC in terms of S-parameters for a two-port antenna is represented in Equation (1), and Equation (2) is a representation of ECC measurement using far-field radiation patterns.

$$\rho_{ij} = \frac{-\sum_{n=1}^{N} S_{ni}^{*} S_{nj}}{\sqrt{\left(1-\sum_{n=1}^{N}|S_{ni}|^{2}\right)\left(1-\sum_{n=1}^{N}|S_{nj}|^{2}\right)}} \tag{1}$$

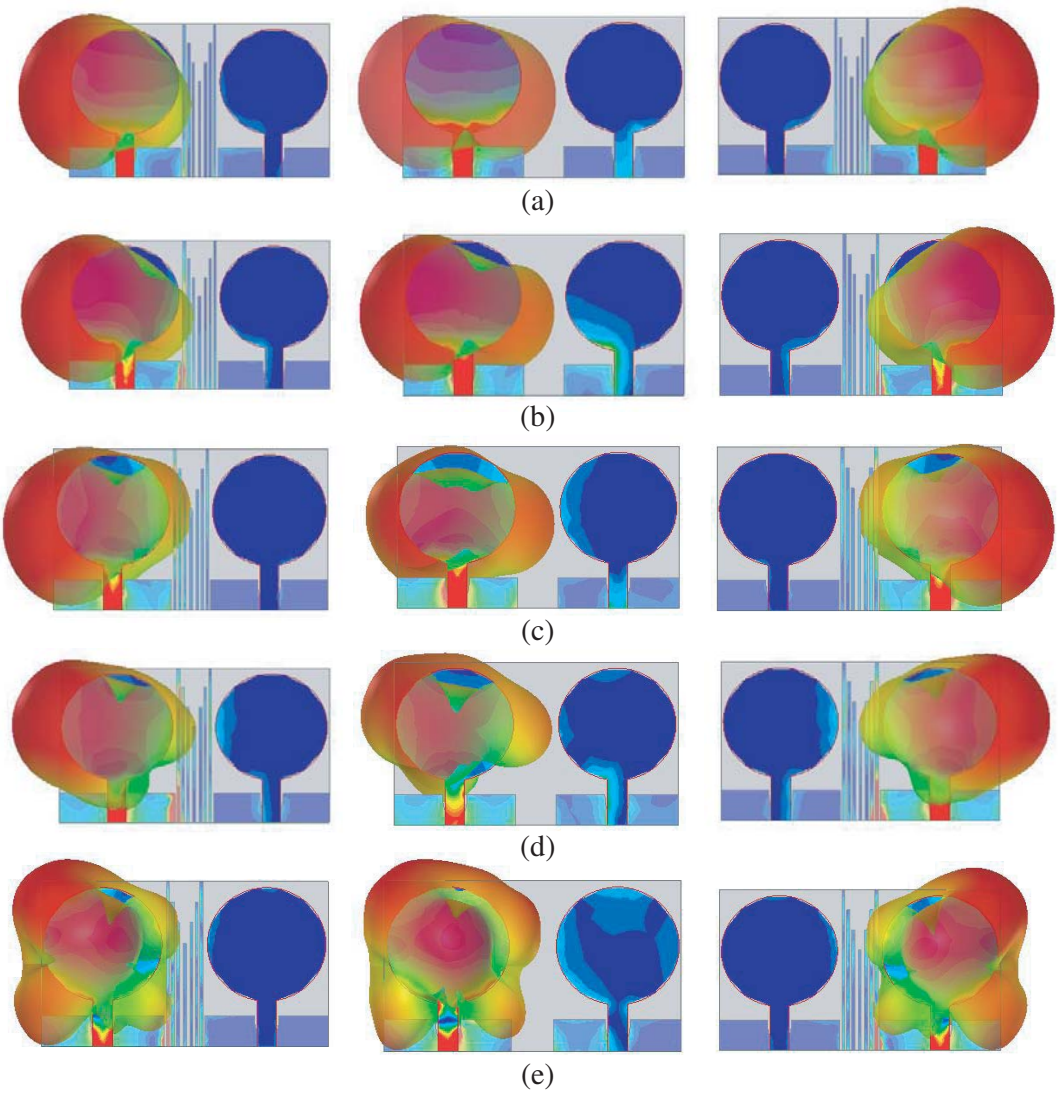

Figure 10. Surface current distribution with 3-D polar plots; (a) at 3.8 GHz; (b) at 6.0 GHz; (c) at 8.0 GHz; (d) at 10.0 GHz; and (e) at 13.6 GHz.

where ρ_{ij} is the correlation between the ith and jth elements of the 'N' element antenna system. For two-port system, it is represented as

$$\text{ECC} = \frac{\left|S_{11}^{*}S_{12} + S_{21}^{*}S_{22}\right|^{2}}{\left(1 - \left|S_{11}\right|^{2} - \left|S_{21}\right|^{2}\right)\left(1 - \left|S_{22}\right|^{2} - \left|S_{12}\right|^{2}\right)}$$

$$\text{ECC} = \frac{\left|\iint \left[\vec{F}_i\left(\theta,\phi\right) \cdot \vec{F}_j\left(\theta,\phi\right)\right] d\Omega\right|^{2}}{\iint \left|\vec{F}_i\left(\theta,\phi\right)\right|^{2} d\Omega \cdot \iint \left|\vec{F}_j\left(\theta,\phi\right)\right|^{2} d\Omega} \tag{2}$$

where $\vec{F}_i$ and $\vec{F}_j$ are the ith and jth antenna radiated fields. The simulated ECC and DG are plotted in Figure 12. The proposed structure has favorable ECC values, which are below 0.04 (acceptable practical value is below 0.5).

The diversity gain (DG) of a two-port MIMO antenna is represented in Equation (3) in terms of ECC and is depicted in Figure 12. The maximum value of DG for the MIMO system is 10 dB. The

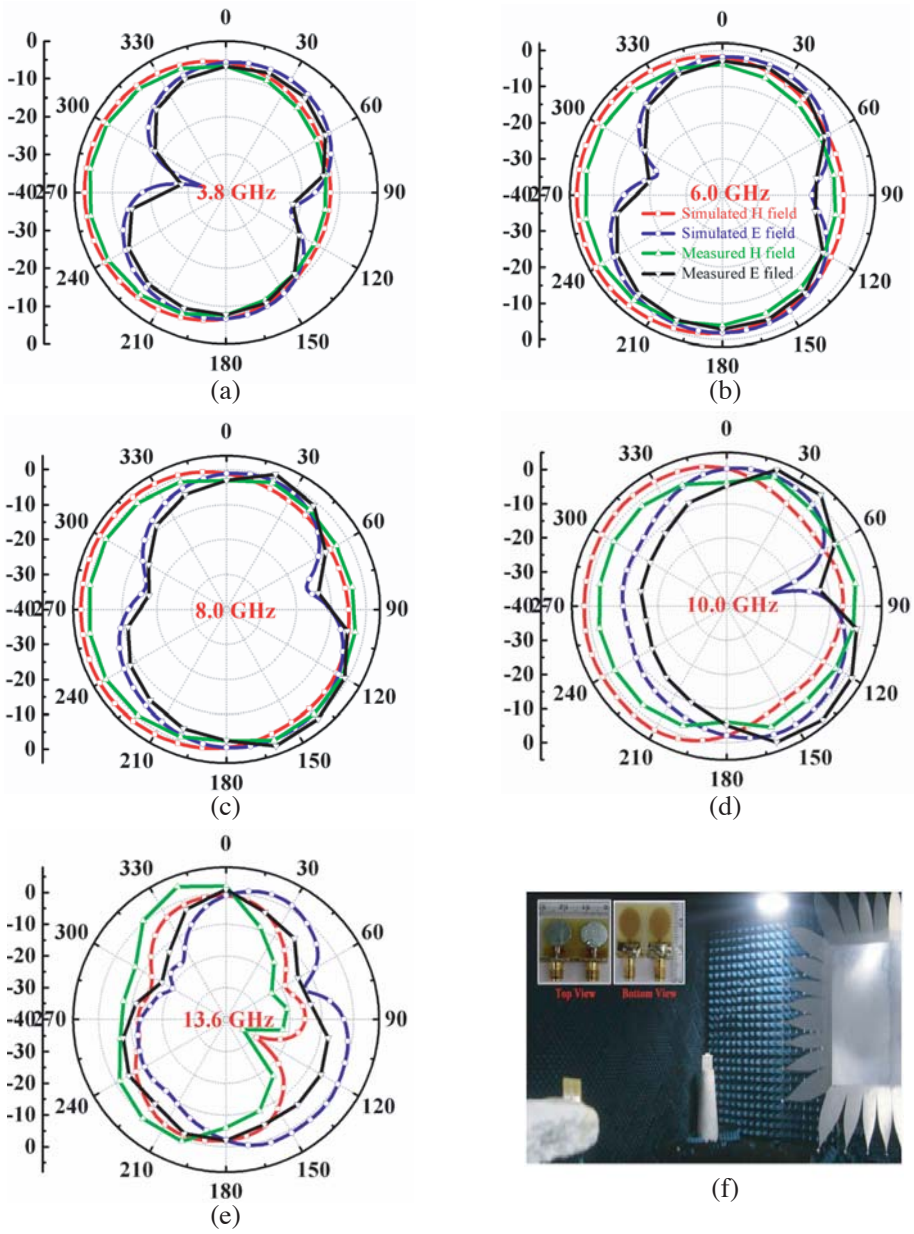

Figure 11. 2-D Radiation patterns (E and H fields); (a) at 3.8 GHz; (b) at 6.0 GHz; (c) at 8.0 GHz; (d) at 10.0 GHz; (e) at 13.6 GHz; and (f) Photograph from anechoic chamber.

proposed structure gives DG values above 9.996 dB in the complete band. From Figure 12, it is observed that the proposed structure provides a good diversified performance.

$$\mathrm{DG} = 10\sqrt{1 - \mathrm{ECC}^2} \tag{3}$$

In MIMO technology, multiple antennas are placed side by side with a smaller distance at the transmitting and receiving ends for compact device applications. Due to a smaller distance, the radiation of one antenna will affect the parameters of the adjacent antenna. The '$S11$' or '$S22$' of individual antennas does not give faithful results. So, a new term is introduced for the reflection coefficient of the whole system named TARC [30, 31]. It considers the changes in self impedances and mutual impedances between individual antennas. TARC is defined in equation (4), and it is represented in terms of S-parameters for the 'N' elements in Equation (5). Figure 13 shows the comparison (simulated and

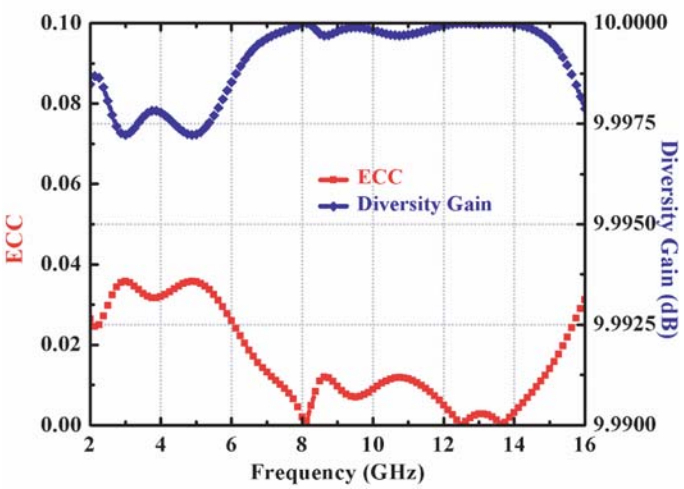

Figure 12. Simulated ECC and DG values.

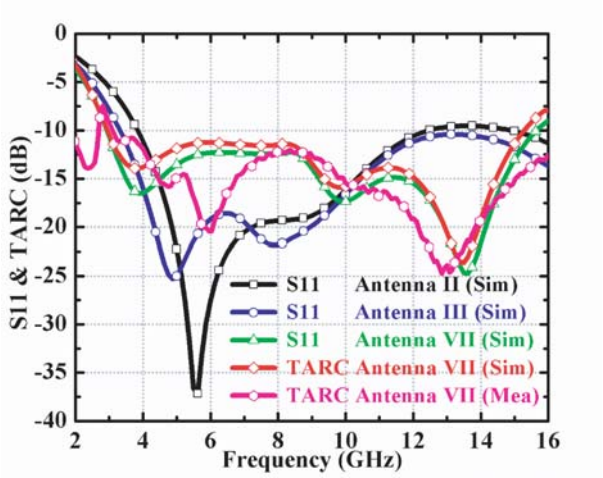

Figure 13. Simulated & measured $S11$ and TARC values.

measured results) of $S11$ values of antennas II, III, and $S11$ & TARC values of the proposed structure. The acceptable values of TARC are less than or equal to '0' dB. The simulated and measured TARC values of the proposed structure are below -10 dB for the entire band.

$$\Gamma_a^t = \sqrt{\frac{available\ power - radiated\ power}{available\ power}} = \sqrt{\frac{P_a - P_r}{P_a}} \tag{4}$$

$$\Gamma_a^t = \frac{\sqrt{\sum_{i=1}^{N} |b_i|^2}}{\sqrt{\sum_{i=1}^{N} |a_i|^2}}, \tag{5}$$

where 'ai' is the ith port forward wave amplitude, $[b] = [S][a]$. For two-port antenna system, it is represented as

$$\text{TARC} = \sqrt{\frac{(S_{11} + S_{12})^2 + (S_{21} + S_{22})^2}{2}}$$

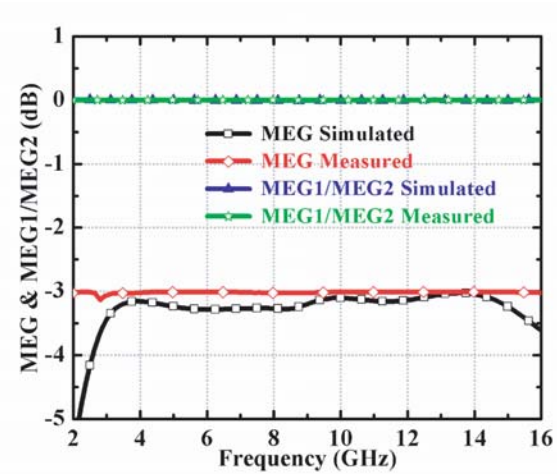

Figure 14. Simulated & measured MEG and MEG1/MEG2 values.

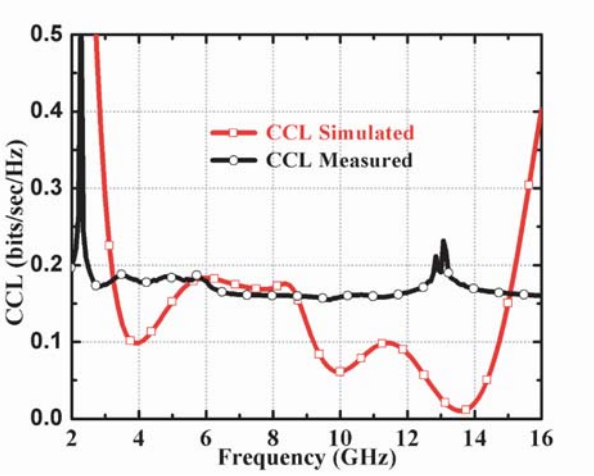

Figure 15. Simulated & measured channel capacity loss (CCL) values.

Mean effective gain (MEG) and MEG ratio are essential parameters for estimating the diversity performance of the MIMO antenna, which are given in Equations (6), (7), and (8). Figure 14 shows the simulated and measured results of MEG (mean effective gain) and MEG1/MEG2. The proposed structure gives required MEG and MEG ratio values, which are around −3 dB and '0' dB, respectively. The channel capacity losses mainly depend on the transmission coefficient values of the MIMO structure. The CCL equation in terms of reflection coefficients ('$S11$' and '$S22$') and transmission coefficients ('$S12$' and '$S21$') for the two-element system are given in Equation (9). The structure has high isolation values above 25 dB in most of the band. Hence, the proposed structure has low values of channel capacity losses, and these are below 0.2 bits/sec/Hz for the entire band, as shown in Figure 15.

$$\mathrm{MEG}_1 = 1 - |S_{11}|^2 - |S_{12}|^2 \tag{6}$$

$$\mathrm{MEG}_2 = 1 - |S_{22}|^2 - |S_{21}|^2 \tag{7}$$

$$\frac{\mathrm{MEG}_1}{\mathrm{MEG}_2} = \frac{1 - |S_{11}|^2 - |S_{12}|^2}{1 - |S_{22}|^2 - |S_{21}|^2} \tag{8}$$

$$\mathrm{CCL} = -\log_2\left[\left(\left(1 - |S_{11}|^2 - |S_{12}|^2\right)\left(1 - |S_{22}|^2 - |S_{21}|^2\right)\right) - \left(\left(S_{11}^* S_{12} + S_{21}^* S_{22}\right)\left(S_{22}^* S_{21} + S_{12}^* S_{11}\right)\right)\right] \tag{9}$$

The performance comparisons of the proposed structure with other structures in terms of antenna electrical size, impedance bandwidth, isolation, peak gain, radiation efficiency, ECC, and TARC are

Table 1. Performance comparison of the proposed structure with other structures.

Reference	Antenna Size (In terms of λ_0)	Impedance bandwidth (GHz)	Isolation (Most of the band) (dB)	Peak gain (dB)	Radiation efficiency (%)	ECC	TARC (dB)	Applications
Issac et al. [3]	$0.37\lambda_0 \times 0.64\lambda_0$	1.6–4	≥ 20	3.8	-	-	-	Wi-Fi, WiMAX
Radhi et al. [4]	$0.48\lambda_0 \times 0.96\lambda_0$	3.1–10.6	≥ 31	3.5 dBi	≥ 75	−29 dB	-	UWB
Qinlong, et al. [5]	$0.31\lambda_0 \times 0.33\lambda_0$	1.56–2.71 & 4.82–5.90	≥ 15	-	≥ 80	0.04	-	GPS

Qian et al. [6]	$0.50\lambda_0 \times 0.60\lambda_0$	3–6	≥ 21	-	-	-	-	Lower UWB
Hao, et al. [7]	$0.35\lambda_0 \times 0.35\lambda_0$	2.3–13	≥ 20	$3-6.1$	-	0.2	-	UWB
Lili et al. [8]	$0.35\lambda_0 \times 0.50\lambda_0$	3–11	≥ 25	> 3	≥ 80	0.004	-	UWB
Amjad et al. [9]	$0.69\lambda_0 \times 0.82\lambda_0$	5.61–5.93	≥ 20	-	-	0.1	-	WiMAX
Amjad et al. [10]	$0.25\lambda_0 \times 0.41\lambda_0$	2.5–14.5	≥ 20	0.3–4.3	-	0.04	-	UWB
Park et al. [11]	$0.35\lambda_0 \times 0.36\lambda_0$	3–9	≥ 17	1–5.5 dBi	≥ 87	0.02	-	UWB
Zhu et al. [12]	$0.35\lambda_0 \times 0.35\lambda_0$	3–12	≥ 20	-	-	0.40	-	UWB
Deng et al. [13]	$0.30\lambda_0 \times 0.41\lambda_0$	3.1–10.6	≥ 16	-	≥ 70	0.15	-	UWB
Zhang et al. [14]	$0.34\lambda_0 \times 0.36\lambda_0$	3.1–5	≥ 22	-	-	-	-	Lower UWB
Ankan, et al. [15]	$0.17\lambda_0 \times 0.23\lambda_0$	2–10. 6	≥ 22	> 3.5 dBi	-	0.2	-	UWB
Mchbal, et al. [16]	$0.26\lambda_0 \times 0.32\lambda_0$	3.1–11.1	≥ 20	-	-	0.002	-	UWB
Rohit, et al. [17]	$0.20\lambda_0 \times 0.40\lambda_0$	3–11	≥ 15	1.5–5	≥ 80	0.8	-	UWB
Liu et al. [18]	$0.22\lambda_0 \times 0.37\lambda_0$	3.1–11	≥ 15	1–5 dBi	≥ 70	0.1	-	UWB
Rohit, et al. [19]	$0.20\lambda_0 \times 0.35\lambda_0$	3.1–11	≥ 20	3–4	≥ 75	0.2	-	UWB
Li et al. [20]	$0.25\lambda_0 \times 0.25\lambda_0$	2.9–11.6	≥ 16	0–6 dBi	-	0.02	-	UWB
Prashant et al. [21]	$0.61\lambda_0 \times 0.77\lambda_0$	8.0–11.5	≥ 20	-	≥ 85	~ 0	≤ -10	Upper UWB
Chandel et al. [22]	$0.16\lambda_0 \times 0.33\lambda_0$	2.8–20	≥ 20	1.6–6	-	0.02	≤ -10	UWB X band and Ku
Chandel et al. [23]	$0.17\lambda_0 \times 0.32\lambda_0$	2.9–20	≥ 20	0–7	≥ 75	0.01	≤ -20	UWB X band and Ku
Aziz et al. [24]	$0.36\lambda_0 \times 0.47\lambda_0$	5.19–5.41 & 7.30–7.66	≥ 22.5	-	≥ 79.8	0.13 & 0.002	≤ -10	WLAN & X band
Ling et al. [25]	$0.21\lambda_0 \times 0.27\lambda_0$	3.1–11	≥ 15	1–3	≥ 70	0.03	-	UWB
Tao et al. [26]	$0.18\lambda_0 \times 0.23\lambda_0$	3–12.4	≥ 20	4	≥ 70	0.1	-	UWB
Anil et al. [27]	$0.14\lambda_0 \times 0.24\lambda_0$	2.87–17	≥ 21	0–6	-	0.01	≤ -20	UWB X band and Ku
Proposed	$\mathbf{0.15\lambda_0 \times 0.27\lambda_0}$	2.95–15.65	≥ 25	1.2–6.8	≥ 90	0.04	≤ -10	UWB X band and Ku

tabulated in Table 1. It is found that the proposed structure has several advantages like very compact size, wide impedance bandwidth, high isolation and radiation efficiency, low ECC, and good TARC values.

5. CONCLUSIONS

A compact UWB-MIMO antenna with high isolation using parasitic reflectors is presented in this communication. The overall structure size is $0.15\lambda_0 \times 0.27\lambda_0$ and consists of two ellipse-shaped radiators with parasitic strips which are used for isolation enhancement. The results demonstrate that the proposed structure operates from 2.95 to 15.65 GHz with good impedance matching. The high isolation of greater than 25 dB is attained in most of the band with the inclusion of parasitic strips between the elements. Also, the peak gain values of 1.2–6.8 dB and radiation efficiency values of above 90% are achieved. It also offers low ECC (< 0.04), high DG (> 9.996 dB), satisfactory TARC (≤ -10 dB), MEG (~ -3 dB), and CCL (0.2 bits/sec/Hz). Thus, the proposed structure is suitable for UWB, X band, and Ku band applications.

ACKNOWLEDGMENT

The authors would like to forward forthright gratitude to Rakesh Kumar Singh, Scientist 'F' and Head, Stealth technologies and test ranges, Directorate of radar seekers and systems (DRSS), RCI, DRDO, Hyderabad, India for giving lab facilities for experimentation and measure the radiation patterns of the fabricated antenna as a segment of research work.

REFERENCES

1. Nadeem, I. and D.-Y. Choi, "Study on mutual coupling reduction technique for MIMO antennas," *IEEE Access*, Vol. 7, 563–586, 2019, DOI: 10.1109/ACCESS.2018.2885558.
2. Malviya, L. and K. Machavaram, "MIMO antennas with diversity and mutual coupling reduction techniques: A review," *International Journal of Microwave and Wireless Technologies*, Vol. 9, No. 8, 1763–1780, 2017, DOI: 10.1017/S1759078717000538.
3. Isaac, A. A., H. Al-Rizzo, S. Yahya, A. Al-Wahhamy, and S. Abushamleh, "Decoupling of two closely-spaced planar monopole antennas using two novel printed-circuit structures," *Microwave Optical Technology Letters*, Vol. 60, No. 12, 2954–2963, 2018, DOI: 10.1002/mop.31405.
4. Radhi A. H., R. Nilavalan, Y. Wang, H. S. Al-Raweshidy, A. A. Eltokhy, and N. Ab Aziz, "Mutual coupling reduction with a wideband planar decoupling structure for UWB-MIMO antennas," *International Journal of Microwave and Wireless Technologies*, Vol. 10, No. 10, 1143–1154, 2018, DOI:10.1017/S1759078718001010.
5. Li, Q., M. Abdullah, and X. Chen, "Defected ground structure loaded with meandered lines for decoupling of dual-band antenna," *Journal of Electromagnetic Waves and Applications*, Vol. 33, No. 13, 1764–1775, 2019, DOI: 10.1080/09205071.2019.1643261.
6. Li, Q., A. P. Feresidis, M. Mavridou, and P. S. Hall, "Miniaturized double layer EBG structures for broadband mutual coupling reduction between UWB monopoles," *IEEE Transactions on Antennas and Propagation*, Vol. 63, No. 3, 1168–1171, 2015, DOI: 10.1109/TAP.2014.2387871.
7. Hu, H. and Z. Lu, "A compact UWB-MIMO antenna for portable applications," *Journal of Electromagnetic Analysis and Applications*, Vol. 8, 240–246, 2016, DOI: 10.4236/jemaa.2016.810022.
8. Wang, L., Z. Du, H. Yang, R. Ma, Y. Zhao, X. Cui, and X. Xi, "Compact UWB-MIMO antenna with high isolation using fence-type decoupling structure," *IEEE Antennas and Wireless Propagation Letters*, Vol. 18, No. 8, 1641–1645, 2019, DOI: 10.1109/LAWP.2019.2925857.
9. Iqbal, A., O. A. Saraereh, A. Bouazizi, and A. Basir, "Metamaterial-based highly isolated MIMO antenna for portable wireless applications," *Journal of Electronics*, Vol. 7, No. 10, 1–8, 2018, DOI: 10.3390/electronics7100267.

10. Iqbal, A., O. A. Saraereh, A. Ahmad, and S. Bashir, "Mutual coupling reduction using F-shaped stubs in UWB-MIMO antenna," *IEEE Access*, Vol. 6, 2755–2759, 2017, DOI: 10.1109/ACCESS.2017.2785232.
11. Park, J.-D., M. U. Rahman, and H. N. Chen, "Isolation enhancement of wideband MIMO array antennas utilizing resistive loading," *IEEE Access*, Vol. 7, 81020–81026, 2019, DOI: 10.1109/Access.2019.
12. Zhu, J., S. Li, B. Feng, L. Deng, and S. Yin, "Compact dual-polarized UWB quasi-self-complementary MIMO/diversity antenna with band-rejection capability," *IEEE Antennas and Wireless Propagation Letters*, Vol. 15, 905–908, 2016, DOI: 10.1109/LAWP.2015.2479622.
13. Deng, J.-Y., L.-X. Guo, and X.-L. Liu, "An ultra wideband MIMO antenna with a high isolation," *IEEE Antennas and Wireless Propagation Letters*, Vol. 15, 182–185, 2016, DOI: 10.1109/LAWP.2015.2437713.
14. Zhang, S. and G. F. Pedersen, "Mutual coupling reduction for UWB-MIMO antennas with a wideband neutralization line," *IEEE Antennas and Wireless Propagation Letters*, Vol. 15, 166–169, 2015, DOI: 10.1109/LAWP.2015.2435992.
15. Bhattacharya, A., B. Roy, S. K. Chowdhury, K. Anup, and Bhattacharjee, "An isolation enhanced, printed, low-profile UWB-MIMO antenna with unique dual band-notching features for WLAN and WiMAX," *IETE Journal of Research*, 1–8, 2019, DOI: 10.1080/03772063.2019.1612284.
16. Mchbal, A., N. Amar Touhami, H. Elftouh, and A. Dkiouak, "Mutual coupling reduction using a protruded ground branch structure in a compact UWB owl-shaped MIMO antenna," *International Journal of Antennas and Propagation*, 1–10, 2018, DOI: 10.1155/2018/4598527.
17. Mathur, R. and S. Dwari, "A compact planar reconfigurable UWB-MIMO antenna with on-demand WiMAX/WLAN rejection," *IET Microwaves, Antennas Propagation*, Vol. 13, No. 10, 1684–1689, 2019, DOI: 10.1049/iet-map.2018.6048.
18. Liu, L., S. W. Cheung, and T. I. Yuk, "Compact MIMO antenna for portable UWB applications with band-notched characteristic," *IEEE Transactions on Antennas and Propagation*, Vol. 63, No. 5, 1917–1924, 2015, DOI: 10.1109/TAP.2015.2406892.
19. Mathur, R. and S. Dwari, "A compact UWB-MIMO with dual grounded CRR for isolation improvement," *International Journal of RF and Microwave Computer-aided Engineering*, 1–9, 2018, DOI: 10.1002/mmce.21500.
20. Li, Z., C. Yin, and X. Zhu, "Compact UWB MIMO vivaldi antenna with dual band-notched characteristics," *IEEE Access*, Vol. 7, 38696–38701, 2019, DOI: 10.1109/ACCESS.2019.
21. Chaudhary, P., A. Kumar, and B. K. Kanaujia, "A low-profile wideband circularly polarized MIMO antenna with pattern and polarization diversity," *International Journal of Microwave and Wireless Technologies*, 1–7, 2019, DOI: 10.1017/S175907871900134X.
22. Chandel, R., A. K. Gautam, and K. Rambabu, "Design and packaging of an eye-shaped multiple-input-multiple-output antenna with high isolation for wireless UWB applications," *IEEE Transactions on Components, Packaging and Manufacturing Technology*, Vol. 8, No. 4, 635–642, 2018, DOI: 10.1109/TCPMT.2018.2806562.
23. Chandel, R., A. K. Gautam, and K. Rambabu, "Tapered fed compact UWB-MIMO-diversity antenna with dual band-notched characteristics," *IEEE Transactions on Antennas and Propagation*, Vol. 66, No. 4, 1677–1684, 2018, DOI: 10.1109/TAP.2018.2803134.
24. Dkiouak, A., A. Zakriti, and M. El Ouahabi, "Design of a compact dual-band MIMO antenna with high isolation for WLAN and X-band satellite by using orthogonal polarization," *Journal of Electromagnetic Waves and Applications*, 1–14, 2019, DOI: 10.1080/09205071.2019.1657504.
25. Wu, L., H. Lyu, and H. Yu, "A novel compact UWB-MIMO antenna with quintuple notched-band characteristics," *Wireless Personal Communications*, Vol. 108, No. 3, 1827–1840, 2019, DOI: 10.1007/s11277-019-06498-5.
26. Tao, J. and Q. Feng, "Compact ultra wideband MIMO antenna with half-slot structure," *IEEE Antennas and Wireless Propagation Letters*, Vol. 16, 792–795, 2017, DOI: 10.1109/LAWP.2016.2604344.

27. Gautam, A. K., A. Saini, N. Agrawal, and N. Z. Rizvi, "Design of a compact protrudent-shaped ultra-wideband multiple-input-multiple-output/diversity antenna with Band-rejection capability," *International Journal of RF and Microwave Computer-aided Engineering*, 1–11, 2019, DOI: 10.1002/mmce.21829.
28. Ray, K. P., "Design aspects of printed monopole antennas for ultra-wide band applications," *International Journal of Antennas and Propagation*, 1–8, 2008, DOI: 10.1155/2008/713858.
29. Sharawi, M. S., A. T. Hassan, and M. U. Khan, "Correlation coefficient calculations for MIMO antenna systems: A comparative study," *International Journal of Microwave and Wireless Technologies*, Vol. 9, No. 10, 1991–2004, 2017, DOI:10.1017/S1759078717000903.
30. Manteghi, M. and Y. Rahmat-Samii, "Multiport characteristics of a wideband cavity backed annular patch antenna for multi polarization operations," *IEEE Transactions on Antennas and Propagation*, Vol. 53, No. 1, 466–474, 2005, DOI: 10.1109/TAP.2004.838794.
31. Addepalli, T. and V. R. Anitha, "Design and parametric analysis of hexagonal shaped MIMO patch antenna for S-band, WLAN, UWB and X-band applications," *Progress In Electromagnetics Research C*, Vol. 97, 227–240, 2019.